Properties of rare-earth iron garnets from first principles

Ryan Nakamoto,[1] Bin Xu,[1,*] Changsong Xu,[1,2] Hu Xu,[3] and L. Bellaiche[1,†]

[1]*Physics Department and Institute for Nanoscience and Engineering, University of Arkansas, Fayetteville, Arkansas 72701, USA*

[2]*State Key Laboratory of Low-Dimensional Quantum Physics and Collaborative Innovation Center of Quantum Matter, Department of Physics, Tsinghua University, Beijing 100084, China*

[3]*Department of Physics, Southern University of Science and Technology, Shenzhen 518055, China*

Structural and magnetic properties of rare-earth iron garnets (RIG), which contain 160 atoms per unit cell, are systematically investigated for rare-earth elements varying from La to Lu (and including Y), by performing spin polarized density-functional calculations. The effects of $4f$ electrons (as core or as valence electrons) on the lattice constant, internal coordinates, and bond lengths are found to be rather small, with these predicted structural properties agreeing rather well with available experiments. On the other hand, treating such electrons as valence electrons is essential to interpret the total magnetization measured in some RIG at low temperature, the different orientation and magnitude of the magnetizations that Fe and rare-earth ions can adopt and to also explain why some RIG have a compensation temperature while others do not. The magnetic exchange couplings and orbital-projected density of states are also reported for two representative materials, namely $Gd_3Fe_5O_{12}$ and $Nd_3Fe_5O_{12}$, when accounting for their $4f$ electrons.

I. INTRODUCTION

As magnetic insulators, rare-earth iron garnets ($R_3Fe_5O_{12}$) or RIG constitute an important class of materials, which are promising for technological applications such as magnetic recording devices with giant magnetorestriction [1], spin Seebeck insulators for thermoelectric generation [2], microwave devices based on current-induced spin torque resonance [3], and Faraday rotators in optical telecommunications [4]. These systems are known to have two different types of Fe ions, namely experiencing a tetrahedral *versus* octahedral coordination environment (Fig. 1), that have been reported to possess magnetic moments that are opposed to each other and of different magnitudes, therefore making RIG ferrimagnetic in nature [4,5]. Moreover, below some characteristic temperature, the rare-earth ions also exhibit a magnetization arising from their $4f$ electrons, and that is commonly believed to align along the magnetization of the octahedral Fe ions [5]. Interestingly, the magnitude of the magnetization of the tetrahedral and octahedral Fe ions, as well as that of R ions, can be strongly temperature dependent, which, e.g., results in the observation of a compensation temperature in some RIGs (but not in others), in which the total magnetic moment crosses the zero value at this specific and material-dependent finite temperature [5,6]. Moreover, since the magnitudes and directions of these three different atomic magnetizations are intrinsically linked to the Faraday effect in RIG [4], it is important to precisely determine such magnetizations.

To the best of our knowledge, very few first-principles studies have been conducted on RIG compounds, probably due to their large primitive unit cell (containing 160 atoms).

For instance, we are only aware of the work of Xu *et al.* about properties of $Y_3Fe_5O_{12}$ (YIG) [7], which is a material that does not possess any f electrons. As a result, several questions remain unanswered. For instance, one may wonder if structural, magnetic, and electronic properties can be well modeled by density-functional theory for a wide range of RIG materials, and if yes, which precise exchange-correlation functional to use. Determining the effects of the ionic radius of the rare-earth ions and of their $4f$ electrons on these properties have also not been accomplished on a computational basis. In particular, can first-principles calculations reproduce the different magnetization's magnitudes and orientations that tetrahedral and octahedral Fe ions and R elements can have and also explain why some RIG compounds have a compensation temperature while others do not? It is also legitimate to ask if the existence of this compensation temperature requires spin-orbit coupling, as similar to the case of the orthoferrites $RFeO_3$ and orthochromites $RCrO_3$ [8] materials, or if one "only" needs to consider collinear magnetism to understand compensation temperatures in RIG.

The goal of this paper is to provide answers to all the aforementioned questions by performing specific density-functional-theoretical calculations on many RIG systems. This paper is organized as follows. Section II provides a description of the computational method used here. Section III reports and discusses the predicted structural, magnetic, and electronic properties of these RIG materials, treating or not the $4f$ electrons of the rare-earth ions as valence electrons. Finally, Sec. IV provides a brief summary of this work.

II. METHODS

Density-functional calculations (DFT) are conducted, via the use of the Vienna *ab initio* simulation package (VASP) [9], in order to investigate rare-earth iron garnets. The generalized gradient approximation (GGA), together with the Perdew-Burke-Ernzerhof (PBE) exchange-correlation functional for solids [10], is employed because of its previous

---

*Author to whom correspondence should be addressed: binxu@uark.edu

†Author to whom correspondence should be addressed: laurent@uark.edu
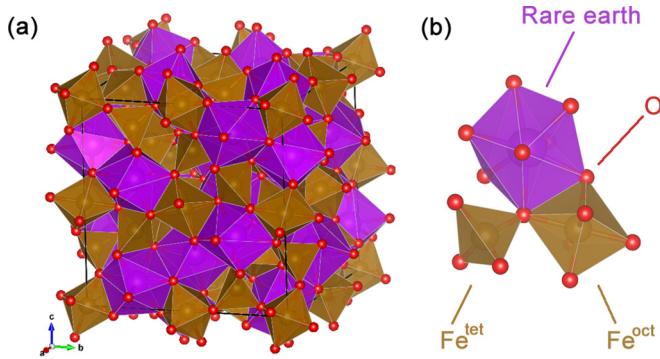
024434-1

FIG. 1. Crystal structure of rare earth iron garnets. (a) Cubic unit cell. (b) Local polyhedra environment experienced by Fe and R ions from their neighboring oxygen ions.

successes in yielding rather accurate structural parameters [11]. The projected augmented wave (PAW) method is used to mimic electron-ion interactions. The localized Fe 3d electrons are treated with an effective Hubbard $U = 4$ eV, as in, e.g., Refs. [11,12], and $U = 0$, 4, or 6 eV is also used for the R ions in cases that their $4f$ electrons are treated as valence electrons as in Refs. [8,13]. The number of valence electrons of Fe ions is eight $(3d^6 4s^2)$ while it is six $(2s^2 2p^4)$ for O ions. Two different types of calculations are performed: type (1) for which the $4f$ electrons of the R ions are considered as core electrons and type (2) for which these electrons are included in the valence. In the first type of calculations, the investigated rare-earth ions are La, Ce, Pr, Nd, Pm, Sm, Gd, Tb, Dy, Y, Ho, Er, Tm, and Lu, with the following electrons being in the valence: La $(5s^2 5p^6 5d^1 6s^2)$, Ce $(5s^2 5p^6 5d^1 6s^2)$, Pr $(5s^2 5p^6 5d^1 6s^2)$, Nd $(5s^2 5p^6 5d^1 6s^2)$, Pm $(5s^2 5p^6 5d^1 6s^2)$, Sm $(5s^2 5p^6 5d^1 6s^2)$, Gd $(5p^6 5d^1 6s^2)$, Tb $(5p^6 5d^1 6s^2)$, Dy $(5p^6 5d^1 6s^2)$, Y $(4s^2 4p^6 4d^1 5s^2)$, Ho $(5p^6 5d^1 6s^2)$, Er $(5p^6 5d^1 6s^2)$, Tm $(5p^6 5d^1 6s^2)$, and Lu $(5p^6 5d^1 6s^2)$. For the second type of calculations, the considered R ions are Ce, Pr, Nd, Pm, Eu, Gd, Tb, Dy, Ho, Er, Tm, Yb, and Lu, and the mimicked valence electrons are Ce $(4f^1 5s^2 5p^6 5d^1 6s^2)$, Pr $(4f^3 5s^2 5p^6 6s^2)$, Nd $(4f^4 5s^2 5p^6 6s^2)$, Pm $(4f^5 5s^2 5p^6 6s^2)$, Eu $(4f^7 5s^2 5p^6 6s^2)$, Gd $(4f^7 5s^2 5p^6 5d^1 6s^2)$, Tb $(4f^9 5s^2 5p^6 6s^2)$, Dy $(4f^{10} 5s^2 5p^6 6s^2)$, Ho $(4f^{11} 5s^2 5p^6 6s^2)$, Er $(4f^{12} 5s^2 5p^6 6s^2)$, Tm $(4f^{13} 5s^2 5p^6 6s^2)$, Yb $(4f^{14} 5s^2 5p^6 6s^2)$, and Lu $(4f^{14} 5s^2 5p^6 5d^1 6s^2)$. Note that we also investigate $Y_3Fe_5O_{12}$ within the type (1) calculations, even if Y is not in the same row of the periodic table as the other investigated rare-earth elements, because of its large technological and fundamental importance [14–16]. Note also that comparing results between type (1) and type (2) will reveal the importance (if any) of the $4f$ electrons of rare-earth ion on properties of $R_3Fe_5O_{12}$. It is also important to know that, unless explicitly specified in the text, the magnetic configuration adopted for the type (2) calculations is such that the magnetization of the rare-earth ions is chosen to be antiparallel to that of the tetrahedral Fe ions while being parallel to that of the octahedral Fe ions—as consistent with a common belief for rare-earth iron garnets [5]. Moreover, the energy cutoff is selected to be 500 eV, and the Monkhorst-Pack k-point mesh is chosen to be $2 \times 2 \times 2$ for the 160-atom cubic unit cell (and $6 \times 6 \times 6$

for the computation of the density of states). Spin-orbit couplings and noncollinear magnetism are not considered in our calculations. Note that all these DFT calculations correspond, of course, to 0 K, but conclusion on the existence of a finite compensation temperature can be drawn from them, as we will see below. Structural optimizations are carried out until the Hellmann-Feynman force on each atom is less than 5 meV/Å. The crystal space group of each investigated compound is identified by the FINDSYM software [17]. It is numerically found to be $Ia\bar{3}d$ for all studied $R_3Fe_5O_{12}$ materials, as consistent with experiments [18].

III. RESULTS

A. Structural properties

The unit cell of such structure is represented in Fig. 1(a), via the use of the VESTA code [19]. As detailed in Fig. 1(b), the Fe ions experience two different types of environments from their neighboring oxygen ions: an octahedral one, with the resulting Fe ions being denoted as Fe^{oct} in the following and occupying the so-called a sites in the Wyckoff positions, *versus* a tetrahedral one, for which the corresponding Fe ions are termed as Fe^{tet} and their Wyckoff positions form the d sites. The ratio between Fe^{oct} and Fe^{tet} is 2:3. On the other hand, all the R ions are dodecahedrally coordinated, and are located on the c sites, while all the O atoms belong to the h sites.

Figure 2 shows the evolution of the predicted cubic lattice parameter, a_{cubic}, of the investigated $R_3Fe_5O_{12}$ materials as a function of the ionic radius (r_R) of their rare-earth element [20] when the $4f$ electrons of R ions are considered as valence electrons, along with the experimental data of Ref. [21]. The effect of the U on R ions, among $U = 0$, 4, and 6 eV, is investigated in this figure, while keeping the U of Fe ions to be 4 eV. The choice of $U = 0$ eV for R gives a better agreement with measurements for small rare-earth ions but disagrees more with experiments for larger R ions. The opposite effect occurs when selecting $U = 6$ eV for R ions. An overall better
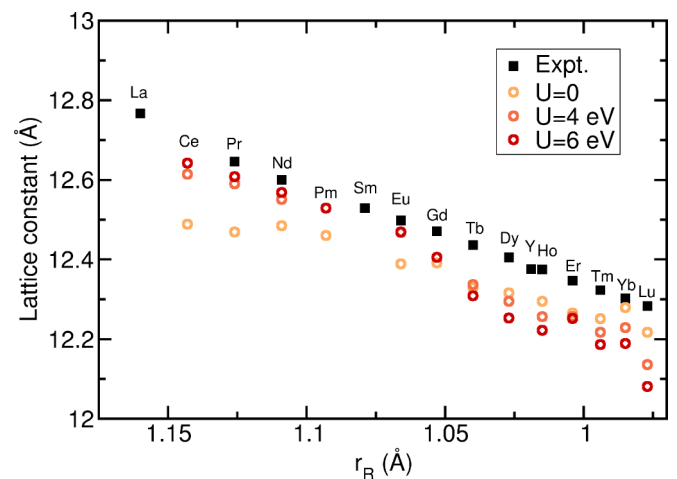

FIG. 2. The cubic lattice constant as a function of the ionic radius r_R from experiment and theory (with $U = 0$, 4, and 6 eV for the R ions) when the $4f$ electrons of the rare-earth ions are considered to be valence electrons. The U for the Fe ions is always equal to 4 eV.
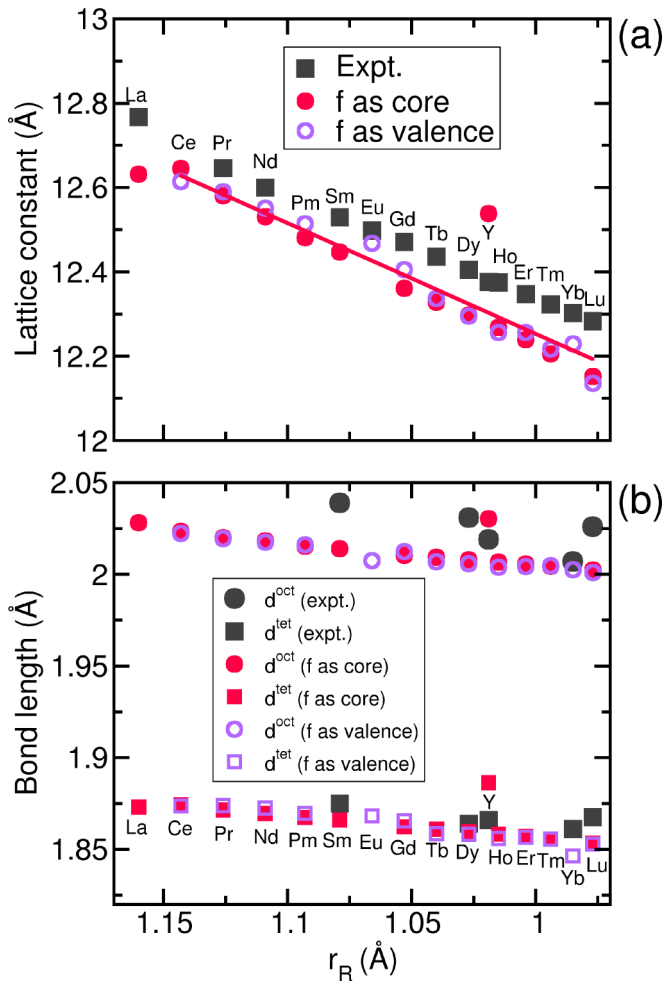
FIG. 3. Variation of (a) the cubic lattice constant and (b) Fe-O bond lengths as a function of the ionic radius, r_R. Dark symbols denote experimental data [21,24]. Symbols report our predictions: red solid dots and squares for the $4f$ electrons of the R ion being treated as core electrons and open purple circles and squares for the $4f$ electrons of R being considered as valence electrons. The solid line is the linear fitting of all the calculated data. Here, $U = 4$ eV is chosen for both the Fe and R ions for the type (2) calculations.

agreement between computations and measurements for all rare-earth ions is rather obtained when choosing the U of R ions to be 4 eV. This latter choice will now be assumed in the following, unless specified. For instance, with this choice of $U = 4$ eV for R, Fig. 3(a) shows the dependence of a_{cubic} on r_R for the two types of calculations conducted here. One can first see that these cubic lattice parameters for the type (1) calculation (i.e., when f electrons of the R ions are treated as core electrons) all nearly linearly decrease when r_R decreases within the Lanthanide series, as consistent with the concept of "chemical pressure" that is typically given to the variation of the rare-earth ionic radius in various R-based families (see, e.g., Refs. [12,22] and references therein). Interestingly, the only element that does not belong to the lanthanide series, that is Y, is predicted to adopt a cubic lattice constant that deviates upward from this linear behavior. Moreover, the inclusion of the $4f$ electrons of R ions in the valence electronic

shell does not seem to qualitatively and even quantitatively affect the linear dependency of a_{cubic} as a function of r_R, as the comparison between the results of types (1) and (2) calculations of Fig. 3(a) reveals. This is consistent with previous works (see, e.g., Ref. [23]) showing the negligible effect of treating these $4f$ electrons as valence, rather than core electrons, on structural properties of other families of rare-earth materials. For instance, considering these $4f$ electrons as valence electrons gives $a_{cubic} = 12.217$, 12.405, and 12.514 Å in $Tm_3Fe_5O_{12}$, $Gd_3Fe_5O_{12}$, and $Pm_3Fe_5O_{12}$, respectively, while treating them as core electrons yield the corresponding values of 12.206, 12.361, and 12.481 Å. Furthermore, our predicted lattice constants agree reasonably well (namely, all within 2%) with the experimental data of Ref. [21]. For instance, the present computations yield $a_{cubic} = 12.632$ and 12.152 Å for $La_3Fe_5O_{12}$ (that has the largest r_R) and $Lu_3Fe_5O_{12}$ (that has the smallest rare-earth ionic radius) within type (1) calculations, respectively, to be compared with the measurements of 12.767 and 12.283 Å. Such agreement attests to the overall accuracy of the calculations.

Table I reports the relaxed internal atomic positions of all studied $R_3Fe_5O_{12}$ compounds, as resulting from the two types of calculations performed here. From these positions and the calculated lattice constants displayed in Fig. 3(a), one can compute the bond lengths between the Fe ions and their nearest O ions, as a function of the rare-earth ionic radius [20]. Such computations are reported in Fig. 3(b) along with the measurements of Ref. [24]. As consistent with experiments, the calculations provide two main sets of data [for both types (1) and (2) calculations] that are both less sensitive in overall to r_R than the cubic lattice constant of Fig. 3(a): The Fe^{oct}-O bonds are typically slightly larger than 2.00 Å while the distance between Fe^{tet} and their nearest O ions is shorter by about 0.15 Å. Figure 3(b) further shows that, like the cubic lattice parameters, (i) our predictions all fall in within 2% of the measurements, with the inclusion or not of the $4f$ electrons into the valence having nearly no effect (note also that Table I reveals that internal coordinates only differ in the fourth digit when including or not the $4f$ electrons in the valence for Pm and Gd, further demonstrating the rather small effect of this inclusion on structural properties); and (ii) the system with $R = Y$ shows the largest deviation from the overall trend (the predicted Fe^{tet}-O bond length is, e.g., significantly larger by ~0.02 Å in $Y_3Fe_5O_{12}$ than in the other rare-earth iron garnets).

B. Magnetic properties

Let us now investigate magnetic properties of rare-earth iron garnets. For the type (1) calculations for which the f electrons are treated as core electrons, the magnetization on R ions is automatically zero (since there are no $4f$ valence electrons that can contribute to the magnetization), which can be thought as corresponding to the experimental situation of a high enough temperature such as the R sublattice is paramagnetic while the Fe sublattice is magnetically ordered. In that case and as reported in Table I, we numerically find that, for any investigated system, each Fe^{oct} ion possesses a magnetic moment of 4.2 μ_B, while each Fe^{tet} ion has an opposite magnetization of around -4.1 μ_B, giving rise to a

TABLE I. Calculated internal coordinates and individual magnetic moments of $R_3Fe_5O_3$. Here, $U = 4$ eV is chosen for both the Fe and R ions for the type (2) calculations.

	internal coordinates				magnetic moments (μ_B)		
R ion	R (24c)	Fe^{tet} (24d)	Fe^{oct} (16a)	O (96h)	R	Fe^{oct}	Fe^{tet}
				f as core			
Y	(1/8,0,1/4)	(3/8,0,1/4)	(0,0,0)	(0.3999,0.3048,0.2230)		4.2	−4.1
La	(1/8,0,1/4)	(3/8,0,1/4)	(0,0,0)	(0.3985,0.3014,0.2197)		4.2	−4.1
Ce	(1/8,0,1/4)	(3/8,0,1/4)	(0,0,0)	(0.3981,0.3022,0.2192)		4.2	−4.1
Pr	(1/8,0,1/4)	(3/8,0,1/4)	(0,0,0)	(0.3985,0.3032,0.2198)		4.2	−4.1
Nd	(1/8,0,1/4)	(3/8,0,1/4)	(0,0,0)	(0.3988,0.3040,0.2204)		4.2	−4.1
Pm	(1/8,0,1/4)	(3/8,0,1/4)	(0,0,0)	(0.3991,0.3047,0.2210)		4.2	−4.1
Sm	(1/8,0,1/4)	(3/8,0,1/4)	(0,0,0)	(0.3994,0.3052,0.2214)		4.2	−4.1
Gd	(1/8,0,1/4)	(3/8,0,1/4)	(0,0,0)	(0.3999,0.3067,0.2223)		4.2	−4.1
Tb	(1/8,0,1/4)	(3/8,0,1/4)	(0,0,0)	(0.4002,0.3072,0.2227)		4.2	−4.1
Dy	(1/8,0,1/4)	(3/8,0,1/4)	(0,0,0)	(0.4004,0.3077,0.2231)		4.2	−4.1
Ho	(1/8,0,1/4)	(3/8,0,1/4)	(0,0,0)	(0.4006,0.3081,0.2234)		4.2	−4.1
Er	(1/8,0,1/4)	(3/8,0,1/4)	(0,0,0)	(0.4008,0.3085,0.2237)		4.2	−4.1
Tm	(1/8,0,1/4)	(3/8,0,1/4)	(0,0,0)	(0.4010,0.3091,0.2241)		4.2	−4.1
				f as valence			
Ce	(1/8,0,1/4)	(3/8,0,1/4)	(0,0,0)	(0.3985,0.3024,0.2200)	0.9	4.2	−4.0
Pr	(1/8,0,1/4)	(3/8,0,1/4)	(0,0,0)	(0.3986,0.3026,0.2204)	2.0	4.2	−4.1
Nd	(1/8,0,1/4)	(3/8,0,1/4)	(0,0,0)	(0.3987,0.3035,0.2206)	2.9	4.2	−4.1
Pm	(1/8,0,1/4)	(3/8,0,1/4)	(0,0,0)	(0.3990,0.3039,0.2210)	4.0	4.2	−4.1
Eu	(1/8,0,1/4)	(3/8,0,1/4)	(0,0,0)	(0.3990,0.3040,0.2216)	6.2	4.1	−4.1
Gd	(1/8,0,1/4)	(3/8,0,1/4)	(0,0,0)	(0.3997,0.3059,0.2221)	7.0	4.2	−4.1
Tb	(1/8,0,1/4)	(3/8,0,1/4)	(0,0,0)	(0.4001,0.3064,0.2227)	6.0	4.2	−4.1
Dy	(1/8,0,1/4)	(3/8,0,1/4)	(0,0,0)	(0.4005,0.3071,0.2234)	5.0	4.2	−4.1
Ho	(1/8,0,1/4)	(3/8,0,1/4)	(0,0,0)	(0.4007,0.3076,0.2238)	4.0	4.2	−4.1
Er	(1/8,0,1/4)	(3/8,0,1/4)	(0,0,0)	(0.4006,0.3079,0.2236)	2.9	4.2	−4.1
Tm	(1/8,0,1/4)	(3/8,0,1/4)	(0,0,0)	(0.4009,0.3088,0.2240)	1.9	4.2	−4.1
Yb	(1/8,0,1/4)	(3/8,0,1/4)	(0,0,0)	(0.4008,0.3079,0.2230)	0.7	4.2	−4.0
Lu	(1/8,0,1/4)	(3/8,0,1/4)	(0,0,0)	(0.4015,0.3100,0.2251)	0.0	4.2	−4.1

total magnetization of 3.69 μ_B per formula unit and an overall *ferrimagnetic* ordering.

When the $4f$ electrons are included as valence electrons, the calculations yield the existence of a magnetization of the R sublattice (M_R), in addition to those of the Fe^{oct} ions ($M_{Fe^{oct}}$) and of the Fe^{tet} ions ($M_{Fe^{tet}}$). The magnetizations of R and Fe are displayed in Fig. 4(a) for each studied $R_3Fe_5O_{12}$ material (for which the $4f$ electrons of the rare-earth ion are treated as valence electrons). Such information is rather important to have, once realizing that extracting each of these three magnetizations from measurements is a rather challenging task while they each play their own role on the value of the Faraday angle that the polarization of light experiences when passing through rare-earth iron garnets [4].

Figure 4(a) and Table I indicate that $M_{Fe^{oct}}$ and $M_{Fe^{tet}}$ are both very close to 4 μ_B per Fe ion in magnitude for any $R_3Fe_5O_{12}$, while M_R adopts a nonmonotonic behavior with r_R: The magnetization of the R ions is vanishing for an empty or full f electronic shell (namely for $R = $ La and Lu) while it adopts a maximum value of 7 μ_B per R ion for the mid-series Gd element, as consistent with the fact that Gd has precisely half-filled $4f$ shells. The nonmonotonic behavior of M_R with the ionic radius of the rare-earth elements explains the "bell curve" shape of our computed 0 K total magnetization (per

formula unit) as a function of r_R displayed in Fig. 4(b) by means of filled red circles, since this total magnetization can be well described by $M_{tot} = 3M_R + 2M_{Fe^{oct}} + 3M_{Fe^{tet}}$ (note that $M_{Fe^{tet}}$ is negative, unlike M_R and $M_{Fe^{oct}}$, and that the oxygen sublattice can also acquire a small magnetization in the calculations).

Another interesting feature can be extracted from the filled red circles of Fig. 4(b), by concentrating on the horizontal line corresponding to 0 μ_B. As a matter of fact, for temperatures for which the Fe ions, unlike the R ions, are already magnetically ordered [6], the total magnetization is only due to Fe ions [as in the case of type (1) calculations] and is thus equal to $2M_{Fe^{oct}} + 3M_{Fe^{tet}}$. It is therefore *negative* according to Table I. Any computational data of Fig. 4(b) being *above* the horizontal line can thus be thought of as indicative that the total magnetization will change its sign from negative to positive when decreasing the temperature, that is when the R ions will first magnetically order and then increase their magnetization. In other words, predicted data above this horizontal line should indicate the existence of a compensation temperature (at which $3M_R + 2M_{Fe^{oct}}$ is precisely opposite to $3M_{Fe^{tet}}$), while data below this line should be representative of a total magnetization that never changes its sign (and thus never annihilates) down to the lowest temperatures. As a
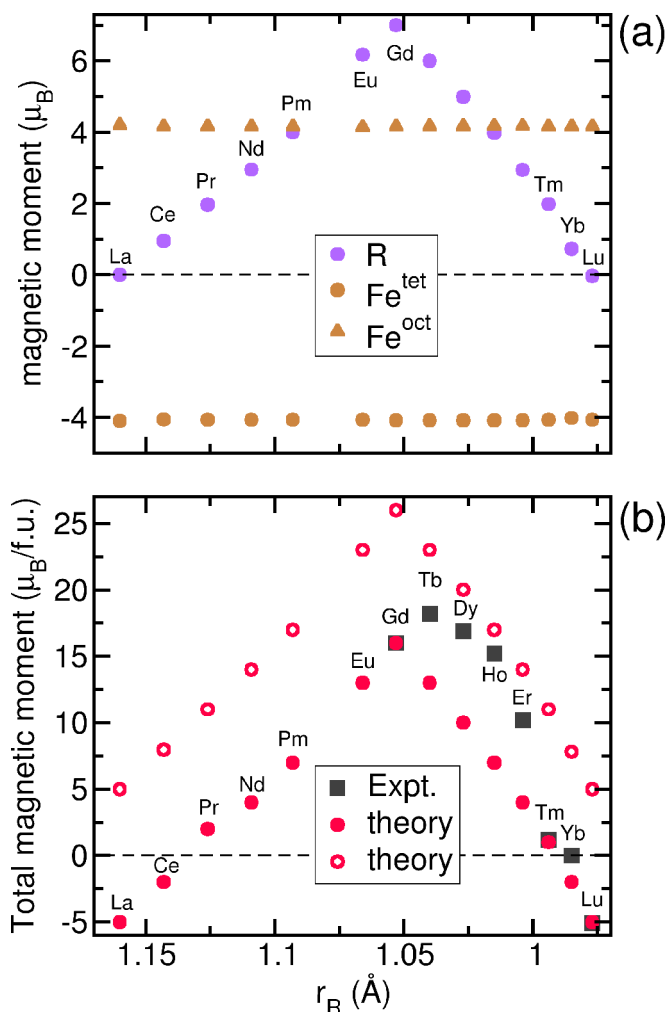
FIG. 4. Variation of (a) the different individual magnetic moments and (b) the total magnetic moment per formula unit as a function of ionic radius r_R. The data of panel (a) and the red circles of panel (b) correspond to the type (2) calculations for which the $4f$ electrons are considered to be valence electrons. The filled red circles are based on the magnetic configuration for which M_R is antiparallel to $M_{Fe^{tet}}$, while parallel to $M_{Fe^{oct}}$. The open circles are based on the magnetic configuration for which M_R is parallel to $M_{Fe^{tet}}$, while antiparallel to $M_{Fe^{oct}}$. The dark gray symbols of panel (b) denote experimental data [6]. Here, $U = 4$ eV is chosen for both the Fe and R ions for the type (2) calculations.
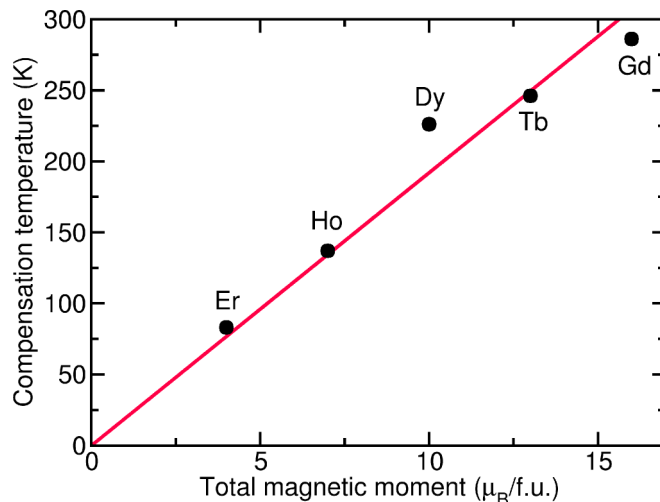

FIG. 5. Correlation between the measured compensation temperatures [6] and the calculated total magnetic moments. These calculations correspond to the case when the magnetization of the rare-earth ions is antiparallel to that of the tetrahedral Fe ions while being parallel to that of the octahedral Fe ions, that is to the filled red circles of Fig. 4(b). The red line is a linear fit passing through the origin, i.e., a 0 K compensation temperature occurs for a zero total magnetic moment. Here, $U = 4$ eV is chosen for both the Fe and R ions for the type (2) calculations.

result, we predict that $R_3Fe_5O_{12}$ with $R =$ Pr, Nd, Pm, Eu, Gd, Tb, Dy, Ho, Er, and Tm will possess a compensation temperature, while those with $R =$ La, Ce, Yb, and Lu will not. Moreover, the stronger positive is the total magnetization at 0 K the higher one can likely expect the compensation temperature to be. Such predictions are consistent with (i) the measurements of Ref. [6] demonstrating the existence of a compensation temperature in $Gd_3Fe_5O_{12}$, $Tb_3Fe_5O_{12}$, $Dy_3Fe_5O_{12}$, $Ho_3Fe_5O_{12}$, and $Er_3Fe_5O_{12}$ and (ii) with the remarkable linear relationship of Fig. 5 we further numerically found between the measured compensation temperatures [6] and the presently calculated total magnetizations associated with the red filled circles of Fig. 4(b). Note also that the straight

line of Fig. 5 passes through the origin, i.e., the compensation temperature is precisely 0 K when $3M_R + 2M_{Fe^{oct}} = 3M_{Fe^{tet}}$ at 0 K. This can explain the very small compensation temperature reported for the Yb compound in Ref. [6]. Note, however, that our calculations indicated by the filled red circles of Fig. 4(b) do not suggest a compensation temperature in $Yb_3Fe_5O_{12}$, which may originate from a slight underestimation of the magnetic moment of Yb in Fig. 4(a). It is also worthwhile to notice that our computations are done on a collinear magnetism level, implying that spin-orbit coupling does not appear to be required to explain the existence of a compensation temperature in $Gd_3Fe_5O_{12}$, $Tb_3Fe_5O_{12}$, $Dy_3Fe_5O_{12}$, $Ho_3Fe_5O_{12}$, and $Er_3Fe_5O_{12}$, which contrasts with the case of the orthoferrites $RFeO_3$ and orthochromites $RCrO_3$ materials [8].

Figure 4(b) also indicates that, while the calculations shown by the filled red circles are in excellent agreement for the Gd and Tm RIGs with the data of Ref. [6] reporting the magnetization measured at 1.4 K, it is not the case for the Tb, Dy, Ho, and Er compounds. As a matter of fact, these calculations largely underestimate the measurements there. We therefore wonder if the magnetic configurations associated with these four latter compounds at low temperature is rather such as M_R is in fact orientated to be antiparallel to $M_{Fe^{oct}}$ while being parallel to $M_{Fe^{tet}}$, to be called "configuration 2" (rather than the common belief that M_R is parallel to $M_{Fe^{oct}}$ while being antiparallel to $M_{Fe^{tet}}$ [5], which is the configuration we chose so far and that we now coined "configuration 1"). To check this hypothesis, Fig. 4(b) further reports, by means of open red circles, our computed total moment of all considered RIGs in configuration 2. The measurements of Ref. [6] much better agree with the (enhanced) magnetic moments of configuration 2 than with those of configuration 1 for

$Tb_3Fe_5O_{12}$, $Dy_3Fe_5O_{12}$, $Ho_3Fe_5O_{12}$, and $Er_3Fe_5O_{12}$, therefore hinting that these latter compounds may adopt configuration 2 at low temperature. Interestingly, configuration 2, unlike configuration 1, cannot give rise to a compensation temperature because the magnetic moment of the rare-earth ions is parallel (rather than antiparallel) to the *net* magnetic moment of the Fe ions, while the experiments of Ref. [6] do report (rather high) compensation temperature in $Tb_3Fe_5O_{12}$, $Dy_3Fe_5O_{12}$, $Ho_3Fe_5O_{12}$, and $Er_3Fe_5O_{12}$. As a result, our computations further suggest that, when cooling these four compounds, the magnetic arrangement is first of configuration 1 type, but then may transform into configuration 2 for a critical temperature that is below the compensation temperature in the samples of Ref. [6]. However, our computed magnetic moments within configuration 2 [that is the open red circles of Fig. 4(b)], in fact, slightly overestimate the low-temperature magnetization of $Tb_3Fe_5O_{12}$, $Dy_3Fe_5O_{12}$, $Ho_3Fe_5O_{12}$, and $Er_3Fe_5O_{12}$ measured in Ref. [6]. This overestimation raises the question whether the samples of Ref. [6] do possess at low temperatures either (i) a *noncollinear* magnetic arrangement (arising, e.g., from spin-orbit coupling) derived from configuration 2 or (ii) exhibit different magnetic domains, such as various domains of configuration 2 having opposite directions for their total magnetization, or even domains of configuration 1 coexisting with domains of configuration 2 (which is a possibility that may be better consistent with the fact that we numerically found that configuration 1 is of lower total energy than configuration 2 in these four systems). In any case, our computations therefore call for new measurements aimed at reexamining the low-temperature magnetic configurations of $Tb_3Fe_5O_{12}$, $Dy_3Fe_5O_{12}$, $Ho_3Fe_5O_{12}$, and $Er_3Fe_5O_{12}$.

Note that the data of Fig. 4 and Table I can also serve as starting points for the computations of other properties. For instance, one can use them to investigate stability of magnetic states and to extract values of magnetic exchange interactions. Let us demonstrate this fact by focusing on four different magnetic configurations for two representative cases, viz., $Gd_3Fe_5O_{12}$ (GIG) and $Nd_3Fe_5O_{12}$ (NIG). These two latter systems are chosen because Gd^{3+} has half filled $4f$ orbitals while Nd^{3+} has three $4f$ electrons (the f orbitals are thus filled less than half). The four magnetic configurations are $\uparrow\uparrow\uparrow$, $\uparrow\uparrow\downarrow$, $\downarrow\uparrow\uparrow$, and $\downarrow\uparrow\downarrow$ for orientations of Fe^{tet}, Fe^{oct}, and R, respectively. In both GIG and NIG, the $\downarrow\uparrow\uparrow$ configuration is numerically found to have the lowest energy, which is consistent with current belief on RIGs [5] and which explains our choice of the magnetic configuration in Table I and Fig. 4(a). Moreover, the $\downarrow\uparrow\downarrow$ configuration is slightly unfavorable with a higher energy of 55 and 69 meV/f.u. than the magnetic ground state for GIG and NIG, respectively, while the two configurations with parallel $M_{Fe^{oct}}$ and $M_{Fe^{tet}}$ have energies that are much higher ($\sim$1 eV/f.u. above the ground state). Once knowing the energies of these four configurations, we can further calculate exchange couplings, using the Heisenberg exchange coupling Hamiltonian $H = E_0 - 2\sum_{i<j}^{N} J_{ij} \boldsymbol{S}_i \cdot \boldsymbol{S}_j$, where N denotes the total number of different $\boldsymbol{S}_i$ and $\boldsymbol{S}_j$ pairs. For RIG, we consider three types of exchange couplings J_{12}, J_{13}, and J_{23}, respectively, between Fe^{tet} and Fe^{oct}, between Fe^{tet} and R, and between Fe^{oct} and R, taking into account the nearest-neighbor interactions with the

following equations:

$$
\begin{aligned}
E_{\uparrow\uparrow\uparrow} &= E_0 - 192 J_{12} S_{Fe^{tet}} S_{Fe^{oct}} - 96 J_{13} S_{Fe^{tet}} S_R \\
&\quad - 192 J_{23} S_{Fe^{oct}} S_R \\
E_{\uparrow\uparrow\downarrow} &= E_0 - 192 J_{12} S_{Fe^{tet}} S_{Fe^{oct}} + 96 J_{13} S_{Fe^{tet}} S_R \\
&\quad + 192 J_{23} S_{Fe^{oct}} S_R \\
E_{\downarrow\uparrow\uparrow} &= E_0 + 192 J_{12} S_{Fe^{tet}} S_{Fe^{oct}} + 96 J_{13} S_{Fe^{tet}} S_R \\
&\quad - 192 J_{23} S_{Fe^{oct}} S_R \\
E_{\downarrow\uparrow\downarrow} &= E_0 + 192 J_{12} S_{Fe^{tet}} S_{Fe^{oct}} - 96 J_{13} S_{Fe^{tet}} S_R \\
&\quad + 192 J_{23} S_{Fe^{oct}} S_R .
\end{aligned}
\tag{1}
$$

Note that each Fe^{tet} has 4 Fe^{oct} and 2 R nearest neighbors, while each Fe^{oct} has 6 R nearest neighbors. The obtained exchange couplings are $J_{12} = -3.71$ meV, $J_{13} = -0.17$ meV, and $J_{23} = +0.05$ meV for GIG, and $J_{12} = -3.71$ meV, $J_{13} = -0.80$ meV, and $J_{23} = -0.02$ meV for NIG. The most significant coupling is therefore between the two types of Fe^{3+} ions, and the coupling is antiferromagnetic in both systems since J_{12} is negative. The magnetic coupling between R^{3+} and Fe^{3+} is much weaker, in particular for that between R and Fe^{oct}, being consistent with the slightly larger distance compared with that between R and Fe^{tet}. Furthermore, the coupling is antiferromagnetic between R and Fe^{tet} since J_{13} is negative too; therefore, M_R is antiparallel to $M_{Fe^{tet}}$, which is (once again) consistent with current belief on RIGs [5] and our choice of the investigated magnetic "configuration 1" of Table I and Fig. 4(a).

C. Electronic properties

Furthermore, we show the calculated density of states (DOS) for $Gd_3Fe_5O_{12}$ and $Nd_3Fe_5O_{12}$ (for the magnetic configuration 1) in Fig. 6, with orbital-projected DOS that illustrate the individual contribution from each type of atom, in particular for two different Hubbard U parameters on the rare-earth ion (that are $U = 0$ and 4 eV) to illustrate their different effect on the electronic properties (while always choosing $U = 4$ eV for Fe ions).

For GIG with $U = 0$ eV for Gd, the band gap is about 1.6 eV. With $U = 4$ eV for Gd, the band gap is very similar to that with $U = 0$ eV, and the partial DOS from O $2p$ and Fe $3d$ orbitals also resemble those with $U = 0$ eV. The main difference between the two cases comes from the Gd $4f$ orbitals: The occupied $4f$ band shifts down in energy and becomes more localized with the finite U, while the unoccupied $4f$ band shifts up. On the other hand, for NIG with $U = 0$ eV, the obtained band gap is only 0.1 eV and the top of the valence band is from the Nd $4f$ states. Such smallness of the gap and associated character of the valence band is likely incorrect, since band gaps of RIGs materials have been measured to be about 2.6 or 2.85 eV [25,26]. By using a finite $U = 4$ eV, the band gap now becomes 1.5 eV, which is more reasonable (when knowing that first-principle calculations can underestimate band gaps by about 1 eV) and that originates from the fact that the occupied $4f$ band shifts down to the energy range of O $2p$ states. Concomitantly the
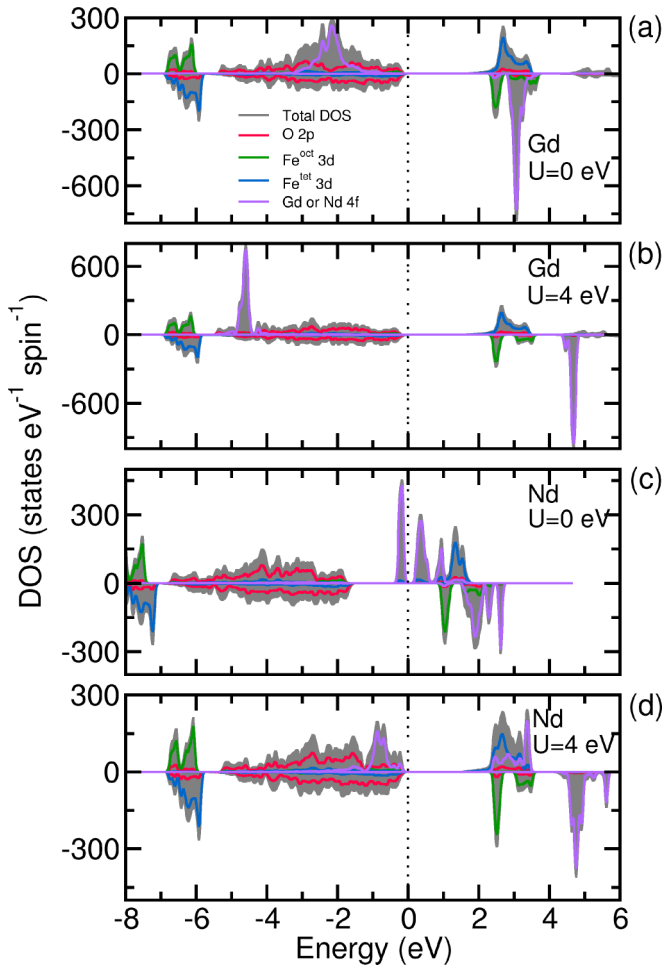
FIG. 6. Calculated total and orbital-projected density of states for the type (2) calculations. The top of the valence band is set to 0 eV, as indicated by the vertical dotted lines. (a) $Gd_3Fe_5O_{12}$ with $U = 0$ eV for Gd ions, (b) $Gd_3Fe_5O_{12}$ with $U = 4$ eV for Gd ions, (c) $Nd_3Fe_5O_{12}$ with $U = 0$ eV for Nd ions, (d) $Nd_3Fe_5O_{12}$ with $U = 4$ eV for Nd ions. Here, $U = 4$ eV is always chosen for Fe ions.

unoccupied $4f$ bands move to higher energies, and the bottom of the conduction band is mostly contributed by the Nd $4f$ and Fe $3d$ orbitals.

Therefore, finite U on Gd only causes a quantitative change of the $4f$ bands in GIG, with relatively minor effect on the band gap, as well as on magnetic properties. The lattice constant also appears to be less affected, as shown in Fig. 2. On the other hand, the effect of U on Nd for NIG is significant, in particular for the nature of the bands around the Fermi energy. The band

gap also closely depends on the magnitude of U, and the lattice constant shows a rather sensitive dependence on U in NIG.

IV. CONCLUSIONS

In summary, we have computationally and systematically investigated structural and magnetic properties of rare-earth iron garnets for R elements varying from La to Lu (and including also Y), with and without $4f$ as valence electrons. Technically, the generalized gradient approximation and the PBE functional for solids [10] was used here, along with the treatment of the localized Fe $3d$ electrons via an effective Hubbard U of 4 eV. In cases that the $4f$ electrons of the R ions were included in the valence, a Hubbard U of 4 eV was also applied to them. The calculated structural results, e.g., lattice constants and bond lengths, are in good agreement with available experimental data, both for the magnitudes and the trend as a function of the rare-earth ionic radius, and are rather insensitive to the inclusion or not of the $4f$ electrons of R ions as valence electrons. On the other hand, this inclusion is crucial to (1) interpret the total magnetization measured in some RIG materials at low temperature, (2) understand the orientation of the magnetic moments of the tetrahedral and octahedral Fe ions and of the R ions, and (3) to also explain (and provide predictions to be checked experimentally) why some RIG compounds have a compensation temperature while others do not. In addition, the effects of the U parameter of R ions on the lattice constant of RIGs and on electronic properties on $Gd_3Fe_5O_{12}$ and $Nd_3Fe_5O_{12}$ materials have been reported, which also demonstrates that the choice of $U = 4$ eV for R ions is appropriate. Our computational results also call for new experiments to precisely determine the low-temperature magnetic configurations of $Tb_3Fe_5O_{12}$, $Dy_3Fe_5O_{12}$, $Ho_3Fe_5O_{12}$, and $Er_3Fe_5O_{12}$.

We thus hope that our predictions are of benefit to the scientific community, even more when realizing that data provided here can also be the starting point for further investigation of other properties of these RIGs, such as phonon spectra, the effect of spin-orbit coupling on the magnetic ground state, computation of Faraday effects, or even temperature evolution of magnetic moments.

ACKNOWLEDGMENTS

[1] F. Sayetat, J. Magn. Magn. Mater. **58**, 334 (1986).

[2] K. Uchida, J. Xiao, H. Adachi, J. Ohe, S. Takahashi, J. Ieda, T. Ota, Y. Kajiwara, H. Umezawa, H. Kawai, G. E. W. Bauer, S. Maekawa, and E. Saitoh, Nat. Mater. **9**, 894 (2010).

[3] M. Schreier, T. Chiba, A. Niedermayr, J. Lotze, H. Huebl, S. Geprägs, S. Takahashi, G. E. W. Bauer, and R. Gross,

and S. T. B. Goennenwein, Phys. Rev. B **92**, 144411 (2015).

[4] W. A. Crossley, R. W. Cooper, and J. L. Page, J. Appl. Phys. **40**, 1497 (1969)

[5] M. Viret, presentation at International School of Oxide Electronics (ISOE2013) Cargèse, France, September 2–14, 2013.

[6] S. Geller, J. P. Remeika, R. C. Sherwood, H. J. Williams, and G. P. Espinosa, Phys. Rev. **137**, A1034 (1965).

[7] Y. N. Xu, Z. Q. Gu, and W. Y. Ching, J. Appl. Phys. **87**, 4867 (2000).

[8] H. J. Zhao, J. Íñiguez, X. M. Chen and L. Bellaiche, Phys. Rev. B **93**, 014417 (2016).

[9] G. Kresse and D. Joubert, Phys. Rev. B **59**, 1758 (1999).

[10] J. P. Perdew, A. Ruzsinszky, G. I. Csonka, O. A. Vydrov, G. E. Scuseria, L. A. Constantin, X. Zhou, and K. Burke, Phys. Rev. Lett. **100**, 136406 (2008).

[11] O. Diéguez, O. E. González-Vázquez, J. C. Wojdel, and J. Íñiguez, Phys. Rev. B **83**, 094105 (2011).

[12] C. Xu, Y. Yang, S. Wang, W. Duan, B. Gu, and L. Bellaiche, Phys. Rev. B **89**, 205122 (2014).

[13] A. Stroppa, M. Marsman, G. Kresse, and S. Picozzi, New J. Phys. **12**, 093026 (2010).

[14] F. F. Y. Wang, Treatise Mater. Sci. Technol. **2**, 279 (1973).

[15] S. Višňovský, R. Krishnan, and V. Prosser, J. Appl. Phys. **49**, 2212 (1978).

[16] Y. Kajiwara, K. Harii, S. Takahashi, J. Ohe, K. Uchida, M. Mizuguchi, H. Umezawa, H. Kawai, K. Ando, K. Takanashi, S. Maekawa, and E. Saitoh, Nature **464**, 262 (2010).

[17] H. T. Stokes and D. M. Hatch, J. Appl. Cryst. **38**, 237 (2005).

[18] S. Geller, Z. Kristallogr. Bd. **125**, 1 (1967).

[19] K. Momma and F. Izumi, J. Appl. Crystallogr. **44**, 1272 (2011).

[20] R. D. Shannon, Acta Crystallogr. A **32**, 751 (1976).

[21] G. P. Espinosa, J. Chem. Phys. **37**, 2344 (1962).

[22] H. Zhao, W. Ren, Y. Yang, X. Chen, and L. Bellaiche, J. Phys.: Condens. Matter **25**, 466002 (2013).

[23] H. J. Zhao, W. Ren, Y. Yang, J. Íñiguez, X. M. Chen, and L. Bellaiche, Nat. Commun. **5**, 4021 (2014).

[24] F. Euler and J. A. Bruce, Acta Crystallogr. **19**, 971 (1965).

[25] A. G. Gavriliuk, V. V. Struzhkin, I. S. Lyubutin, and I. A. Trojan, JETP Lett. **82**, 603 (2005).

[26] R. Metselaar and P. K. Larsen, Solid State Commun. **15**, 291 (1974).